RSC Advances

PAPER

View Article Online
View Journal | View Issue

Cite this: *RSC Adv.*, 2025, **15**, 43426

Synthesis and coordination ability of the first phosphavinyl(selenoxo)phosphorane: an electronic story†

Iulia-Andreea Aghion,[a] Raluca A. Septelean,*[b] David Lucaci,[b] Ionut-Tudor Moraru,[b] Albert P. Soran,[c] Catalin C. Ciocan,[b] Emilia Licarete,[d] Manuela Banciu[d] and Gabriela Nemes*[b]

The Mes*P=C(Cl)–P(=Se)(i-Pr)$_2$ phosphavinyl(selenoxo)phosphorane is the first derivative of this new class of compounds embedding in the same unit a λ^2 P(III) and a λ^4 P(V) atom. This electron-rich compound is a good candidate for new coordination compounds, but also for potential biologic applications. The coordination ability of the phosphavinyl(selenoxo)phosphorane derivative towards transition metals was evaluated by means of both experimental and theoretical analyses. Along with the gold and palladium complexes, we report here the first copper(II) coordination compound stabilised with a phospha(chalcogenoxo)phosphorane type ligand as well as a heterobimetallic gold and copper containing derivative stabilised with two phospha(selenoxo)phosphorane units. Density functional theory (DFT) calculations, coupled with natural bond order (NBO), energy decompostion analysis (EDA) and unrelaxed bond dissociation energy (UBDE) analyses were systematically performed to gain insight into the electronic structure of targeted compounds, and to understand wheter the type of the chalcogen atom influences the coordination behaviour of the P=C–P=(X) moiety (X = O, S or Se). The selenium compound demonstrated no impact on cell viability, while exerting a clear protective effect through the reduction of oxidative stress while the Se–Au compound significantly reduced cell viability in the same experimental setting.

Received 18th July 2025
Accepted 20th October 2025

DOI: 10.1039/d5ra05176b

rsc.li/rsc-advances

Introduction

Unsaturated phosphorus compounds containing a P=C–P unit (phosphavinylphosphoranes) have attracted significant attention due to their distinctive reactivity,[1] and their role as versatile building blocks in organometallic and coordination chemistry.[2] The insertion of heavier chalcogen atoms into their molecular backbone expands the chemical perspective, leading to novel structural motifs of the P=C–P(=X) (X = O, S) type with remarkable electronic properties, given their ability to form coordinate bonds through multiple centres (*i.e.*, P(III) and X atoms or the P=C double bond) with various transition metals.[3–10] Thus, it was highlighted that the coordination behaviour of phosphavinyl(oxo- or thioxo)phosphoanes to gold fragments is strongly influenced by the type of R groups grafted on the P(V) atom, or by the nature of the chalcogen atom, both playing an important role in orienting the coordination towards the P(III) or the chalcogen atom.[11] On the other hand, the coordination to Pd(II) containing fragments, the stabilisation of the resulting compounds is achieved with the activation of the C–H bond of a *t*-Bu group from the 2,4,6-tri-*tert*-butylphenyl (Mes*) and the formation of a 5-member-cycle by its oxidative addition to the P(III)=C unit.[11,13] In this respect, we have previously highlighted in a series of studies[11–14] the great interest for the chemistry of phosphavinyl(oxo- and thioxo) phosphoranes, as electron-rich fragments with great potential for orienting the coordination towards different *p* or *d*-block metals.

The stabilisation of the P=C–P(=X) (X = O, S) moiety is obtained by grafting bulky organic substituents on the λ^2 P(III) atom, with the Mes* group being renowned for providing the required steric hindrance,[15] whereas at the λ^4 P(V) atom, a smaller encumberment is required.[12–14,16] On the other hand, recent studies show that the coordination preferences of P–C=

[a]*Faculty of Chemistry and Chemical Engineering, Doctoral School of Chemistry, Babes-Bolyai University, Cluj-Napoca 400028, Romania*

[b]*Faculty of Chemistry and Chemical Engineering, Department of Chemistry, Babes-Bolyai University, Cluj-Napoca 400028, Romania. E-mail: raluca.septelean@ubbcluj.ro; gabriela.nemes@ubbcluj.ro*

[c]*Faculty of Chemistry and Chemical Engineering, Department of Chemistry, Supramolecular Organic and Organometallic Chemistry Centre (SOOMCC), Babes-Bolyai University, Cluj-Napoca 400028, Romania*

[d]*Faculty of Biology and Geology, Babes-Bolyai University, Cluj-Napoca 400028, Romania*

† In memoriam Ioan Silaghi-Dumitrescu (1950–2009), professor at the Babeș-Bolyai University, Faculty of Chemistry and Chemical Engineering, corresponding member of the Romanian Academy, to mark 75 years from his birth.

P(=X) species through S or P(III) atoms to organometallic fragments can be influenced by the electronic properties of the organic groups grafted to P(V) atom of phosphavinyl(-chalcogenoxo)phosphorane skeleton, at least to the same extent as their steric hindrance.[11] To bring further knowledge to this field, we have expanded our research on a new class of phosphavinyl(selenoxo)phosphoranes. To the best of our knowledge, there are no reported studies providing any information regarding this class of compounds. Moreover, there are only a few reports on derivatives containing a PCP moiety and at least a P=Se chemical bond.[17–21]

In this study we present the synthesis and characterization of a new phosphavinyl(selenoxo)phosphorane derivative, together with its reactions with different transition metals (gold, palladium, copper), and a preliminary study regarding its cytotoxicity. Theoretical investigations are performed to understand the electronic structure and the coordination properties of this species.

Results and discussions

Synthesis, structure, and electronic features of the Mes*P=C(Cl)–P(=Se)(i-Pr)$_2$ derivative

The novel phosphavinyl(selenoxo)phosphorane compound, Mes*P=C(Cl)–P(=Se)(i-Pr)$_2$ **1** was obtained by selective oxidation of the freshly prepared Mes*P=C(Cl)–P(i-Pr)$_2$ compound, which was synthesized by a procedure previously reported by our group,[11] with grey selenium in toluene and was isolated as a yellow crystalline solid from pentane (Scheme 1).

Derivative **1** was completely characterized in solution by multinuclear NMR spectroscopy and HRMS spectrometry. In the ^{31}P NMR spectrum, two doublet signals were observed, one at 69.8 ppm (d, $^{2}J_{P,P}$ = 95.4 Hz) attributed to the P(V) atom and at 336.1 ppm corresponding to the phosphorus atom involved in the P(III)=C unit, respectively, in the expected range for such diphosphaalkenes.[11,13,14,16]

The presence of the selenium atom was confirmed through ^{31}P NMR spectroscopy, by the satellites observed for the signal attributed to the P(V) atom ($^{1}J_{P,Se}$ = 707.9 Hz) and the P(III)=C atom ($^{3}J_{P,Se}$ = 61.3 Hz) and, furthermore, by the doublet of doublets observed in the ^{77}Se NMR spectrum at −408.8 ppm. All the NMR data are presented in the experimental part.

Compound **1** is highly soluble in most solvents and was found to be stable in solid state and in alcohol solutions (MeOH, EtOH) for several days. The solid structure of **1** was confirmed by single crystal X-ray diffraction (see Fig. 1(left) and Table S1 in SI for supplementary crystallographic data). Compound **1** crystallizes in monoclinic space group $P2_1/n$ with one molecule in the asymmetric unit (Fig. 1a). The equivalent bond lengths and angles are very similar to the analogous P=O and P=S compounds,[11,16] and the geometrical parameters are consistent with the double bond character involving the λ^2 P(III) and the λ^4 P(V) phosphorus atom respectively (Table S2). There is an almost antiperiplanar (Se, Cl) arrangement relative to the P1–C1 bond, with Se–P1–C1–Cl1 dihedral angle greater than 160°, similar to those observed for the lighter O and S analogues.

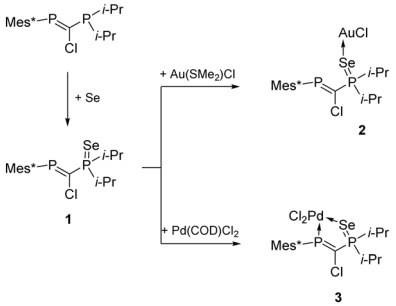

Scheme 1 Synthesis of compound **1** and its coordinative derivatives with Au(SMe$_2$)Cl and Pd(COD)Cl$_2$.

DFT calculations were performed to gain insight into the electronic features of **1**, as well as its counterparts containing P=C–P(=O) and P=C–P(=S) moieties. Even though the latter were explored in previous studies,[11,12] systematic comparisons for an extended series of phosphavinyl(chalcogeno)phosphoranes, in terms of chemical bonding, nucleophilicity, charge distribution, conformational equilibria, and so forth, should allow the rational design of novel compounds incorporating the electron-rich P=C–P(=X) (X = O, S, Se) backbone. Based on the calculations, the optimized molecular structure of **1** is in close agreement with the one measured in the solid-state, in terms of both bond lengths and angles (conformer **1**, Fig. S33). Given that in solution the rotation around the σ(C–P) bond is likely to occur, we also investigate another possible conformation of **1** in which the P(sp^2) and Se atoms are displaced *trans* with respect to the C–P(sp^3) axis (conformer **2**, Fig. S33). Similar DFT analyses were conducted on the lighter Mes*P=C(Cl)–P(=O)(i-Pr)$_2$ and Mes*P=C(Cl)–P(=S)(i-Pr)$_2$ counterparts containing oxygen and sulphur, respectively. The energy difference between the analysed conformers of Mes*P=C(Cl)–P(=X)(i-Pr)$_2$ derivatives (X = O, S, Se) are basically constant for the entire series (Table S5). In all cases, the conformation involving the *cis* orientation of the P(sp^2) and Se atoms, with respect to the C–P(sp^3) axis, is the most stable one. In fact, this conformation resembles the geometry measured in the solid-state for the selenium derivative **1**.

The charges of the atoms contained in the P=C–P(=X) unit of investigated compounds were computed through natural bond orbital (NBO) analyses, for both studied conformers (Table 1). For each conformation the charges on the P(sp^2) and C atoms are hardly affected by the type of X chalcogen atom, yet they are slightly influenced by conformational changes.

Bond orders (BOs) between atoms incorporated within the P=C–P(=X) fragment (X = O, S, Se) were computed in the framework of the NBO analysis. It is shown that the BOs of the P=C and C–P bonds are hardly affected by the type of X atom, as well as the P=X bonds (X = O, S, Se) which exhibit BOs between 1.49 and 1.55 (Table S6).

Coordination properties of Mes*P=C(Cl)–P(=Se)(i-Pr)$_2$ and the Chalcogen Effect in Targeted Complexes.

Compound **1** is particularly interesting due to the presence of multiple coordination sites: the selenium and the phosphorus λ^2 P(III) atoms as well as the C=P double bond, potentially leading to mono-, bi- or tridentate derivatives. To gain

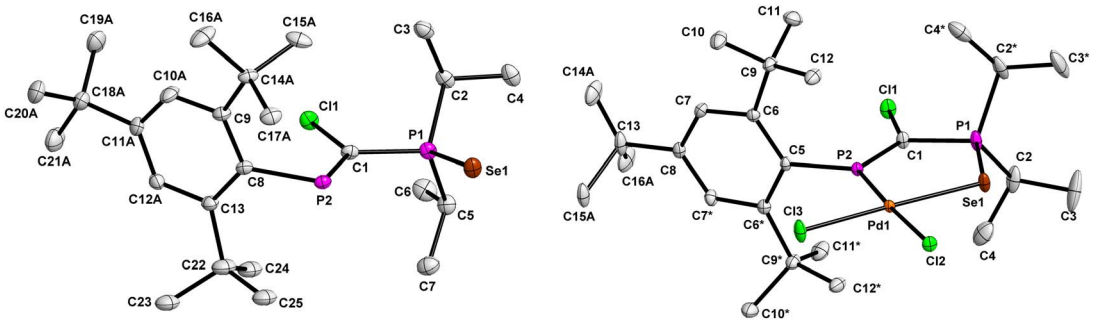

Fig. 1 The asymmetric unit of **1** (Fig. 1-left) and **3** (Fig. 1-right) shown with 30% probability of ellipsoids. Hydrogen atoms are omitted for clarity. **1**: bond length (Å): P1═Se1 2.110(1), P2═C1 1.680(2); angles (°): C1–P1═Se1 110.8(1), P2═C1–P1 119.6(1), Se1═P1–C2(i-Pr) 112.6(1). **3**: bond length (Å): P1═Se1 2.176(1), P2═C1 1.796(3), Pd1–Se1 2.398(1), P2–Pd1 2.203(1); angles (°): C1–P1═Se1 107.3(2), P2═C1–P1 118.6(2), P2–Pd1–Se1 91.6(1).

Table 1 Natural charges computed for the atoms contained in the P═C–P(═X) backbone, for the two conformations investigated for each compound within the Mes*P═C(Cl)–P(═X)(i-Pr)$_2$ (X = O, S, Se) series[a]

P═C–P(═X) backbone	P(III)	C	P(V)	X
Conformer 1(*cis*)				
X = O	0.804	−0.907	1.936	−1.101
X = S	0.819	−0.904	1.351	−0.605
X = Se	0.823	−0.9112	1.255	−0.515
Conformer 2(*trans*)				
X = O	0.717	−0.876	1.930	−1.096
X = S	0.724	−0.866	1.338	−0.600
X = Se	0.727	−0.871	1.241	−0.512

[a] The computed charge on the P(sp^3) atom is highly impacted by the type of X atom (increasing as expected from X = Se to X = O), with no significant differences being noticed between the charges calculated for the two conformers. The charges of the chalcogen atoms are in all cases negative (their absolute values increasing as expected from O toward Se), being hardly impacted by the rotation around the σ(C–P) bond.

more insight into the ability of **1** to coordinate to transition-metals, its reactions with gold and palladium fragments were first examined. By mixing Mes*P═C(Cl)–P(═Se)(i-Pr)$_2$ **1** with Au(SMe$_2$)Cl in dichloromethane, in a 1 : 1 molar ratio, it results immediately into the gold complex {Mes*P═C(Cl)–P(═Se)(i-Pr)$_2$}AuCl **2** (Scheme 1), as a yellow powder. The reaction occurs in a nearly quantitative yield, according to the ^{31}P NMR spectrum recorded for the crude reaction mixture after 30 minutes. The ^{31}P NMR spectrum of **2** shows the presence of two resonance signals, one at 331.4 ppm (d, $^2J_{P,P}$ = 92.0 Hz) for the P(III) atom with additional satellites due to the coupling with selenium atom ($^3J_{P,Se}$ = 71.6 Hz) and the second one for the P(V) atom at 64.1 ppm (d, $^2J_{P,P}$ = 92.0 Hz) with a strong selenium coupling ($^1J_{P,Se}$ = 664.2 Hz). The chemical shifts in the ^{31}P NMR spectrum of compound **2** are very close to the ones observed for the ligand **1**, the only notable difference being the $^1J_{P,Se}$ that decreases by about 50 Hz, suggesting that the gold atom is bonded to the selenium atom (see Scheme 1). In addition, the ^{77}Se NMR spectrum reveals a broad doublet signal at −377.7 ppm. All the RMN data are described in the experimental part.

Due to its low solubility in hydrocarbons, only poor-quality crystals were obtained by slow diffusion. Compound **2** crystallizes as a solvate with one molecule of chloroform (Fig. S19), only a partial solution of the structure could be found in the orthorhombic *Pbca* space group. Some carbon atoms have NPD thermal ellipsoids when refined anisotropically, so the final solution and refinement to convergence could not be completed. However, the X-ray diffraction data affords evidence that in the solid state the Se atom of ligand **1** is coordinated to the Au–Cl fragment. The organic ligand is coordinated to gold only through the selenium atom, resulting in an almost linear coordination geometry at the metal centre. The Se–Au bond length of 2.376(3) Å compares well with statistical values for the similar compounds containing the C$_3$P═Se–Au–Cl structural unit [range 2.369–2.391 Å, and a mean value of 2.375(7) Å] found in the CSD (version 6.00/April 2025). Some geometrical parameters for compound **2** are given in Table S3, however these data should be regarded with some degree of caution due to problems mentioned above. Aurophilic Au⋯⋯Au interactions at 3.209 Å (similarly to reported data[18]) were identified in the crystal structure, which lead to the formation of dimeric units (Fig. S32) and which is in contrast with the analogous complex with the P═S ligand for which no such aurophilic interaction were observed.[11]

DFT investigations were employed to shed light on the structural and electronic properties of **2**, including its coordination behaviour. It is shown that the molecular complex formed *via* the Se → Au bond is with *ca.* 2.5 kcal mol^{-1} more stable than the one involving the P(III) → Au donation (Table S7), reinforcing the crystallographic and ^{31}P NMR findings. By extending this analysis to the homologue series of {Mes*P═C(Cl)–P(═X)(i-Pr)$_2$}AuCl (X = O, S, Se) complexes, we highlight that the coordination preferences of the electron-rich P═C–P(═X) backbone are easily tailored by playing with the type of X chalcogen atom (Table S8). Opposite to the selenium-based complex, the P═C–P(═O) unit favours the formation of P(III) → Au over O → Au bond by >10 kcal mol^{-1}, while for the sulphur counterpart, the narrow energy gap (<1 kcal mol^{-1})

between complexes formed through P(III) → Au or S → Au bonds indicates fluxionality, in line with reported studies on P=C–P(=S) moieties.[11]

The coordination preferences of targeted complexes are further highlighted by evaluating the thermodynamic accessibility of Mes*P=C(Cl)–P(=X)(i-Pr)$_2$ + Au(SMe$_2$)Cl ⇌ {Mes*P=C(Cl)–P(=X)(i-Pr)$_2$}AuCl + SMe$_2$ reaction.

It is emphasized that the spontaneous formation of targeted complexes, involving either P(III) → Au or X → Au bonds, is closely related to the nature of chalcogen atom, given the computed $\Delta_r G°$ values in DCM (Table 2). Thus, the P=C–P(=O) moiety will form stable complexes only *via* the P(III) → Au bond, the P=C–P(=S) unit favours both P(III) → Au and S → Au donations, while the P=C–P(=Se) system spontaneously forms gold complexes merely through the Se → Au bond.

The selective coordination of the gold metal centre was also highlighted in an experimental study, the reaction of **1** with Au(SMe)$_2$Cl in a 1 : 2 molar ratio leads, even after heating, only to the monosubstituted gold complex in which the connection to the gold fragment is obtained *via* the Se atom, similarly to the 1 : 1 molar ratio reaction (see Fig. S10b). The specific signals for P(III) and P(V) atoms in ^{31}P NMR spectra have practically the same values of chemical shift as in the case of compound **2**, while for the gold complexes formed with P=C–P(=S), in which the Au centre is connected to a P(sp^2) atom, the resonance signal for the P(III) atom shifts to 251.1 ppm.[11]

The strength and nature of the X → Au (X = O, S, Se) and P(III) → Au donations are also relevant indicators for the stability of targeted complexes. According to unrelaxed bond dissociation energy (UBDE) calculations (Table S9), the interaction-energy of P(III) → Au is constant (54.5 ± 0.2 kcal mol^{-1}) in all {Mes*P=C(Cl)–P(=X)(i-Pr)$_2$}AuCl complexes, regardless of the chalcogen atom, while the X → Au bond-strength increases considerably from O (42.1 kcal mol^{-1}) to S (53.9 kcal mol^{-1}) and Se (55.0 kcal mol^{-1}). The UBDE values are in very close agreement with bond strengths obtained from the energy decomposition analysis (EDA) scheme (for comparison, see Tables 3 and S9). In addition, the bonding picture derived from EDA calculations suggests for P(III) → Au a predominant covalent character (58–60% in all complexes), while the covalency of X → Au increases from O (42%) to S (53.5%) and Se (54%).

NBO calculations were performed on the entire series of {Mes*P=C(Cl)–P(=X)(i-Pr)$_2$}AuCl complexes, to evaluate the charge distribution within the P(→Au)=C–P = X or the P=C–P = X(→Au) fragments (Table S10). In addition, natural bond orders were computed for the same backbones (Table S11). In comparison to the uncomplexed species (see Table 1 for comparison), the computed BO for the P=C and C=P bonds are only slightly affected by the coordination of the P=C–P(=X) moiety to gold, regardless of whether the complexes were formed *via* the P(III) → Au or the X → Au bond. On the contrary, the P=X bond order is considerably influenced by the formation of the gold complex, especially when it is formed through X → Au donations. Concerning the P(III) → Au bonds, the NBO calculations reveal BOs of *ca.* 0.50 in all cases, while for X → Au the BO increases significantly from O (BO = 0.27) to S (BO = 0.47) and Se (BO = 0.50).

Furthermore, Mes*P=C(Cl)–P(=Se)(i-Pr)$_2$ is a good candidate for obtaining stable chelates. The reaction of **1** with dichloro(1,5-cyclooctadiene)palladium(II) in dichloromethane, in a 1 : 1 molar ration, leads to the new complex {Mes*P=C(Cl)–P(=Se)(i-Pr)$_2$}PdCl$_2$ **3**, which was obtained as orange crystals in toluene/hexane. The near-quantitative formation of complex **3**, was revealed by the ^{31}P NMR of the crude solution. The ^{31}P NMR spectra are consistent with the presence of a sole species. Indeed, two doublet signals were observed for both P(III) atom at 284.0, ($^2J_{P,P}$ = 76.3 Hz) and P(V) atom at 64.1 ($^2J_{P,P}$ = 76.3 Hz, $^1J_{P,Se}$ = 526.2 Hz) while the ^{77}Se NMR spectrum shows a doublet of doublets at −103.2 ppm ($^1J_{P,Se}$ = 526.2 Hz and $^3J_{P,Se}$ = 21.9

Table 2 Calculated $\Delta_r G°$ values for the Mes*P=C(Cl)–P(=X)(i-Pr)$_2$ + Au(SMe$_2$)Cl ⇌ {Mes*P=C(Cl)–P(=X)(i-Pr)$_2$}AuCl + SMe$_2$ reaction, in the case of complexes formed *via* P(III) → Au and X → Au bonds

	Complex formed *via* P(III) → Au bond	Complex formed *via* X → Au bond
X	$\Delta_r G°$ (kcal mol^{-1})	
O	−2.5	10.2
S	−0.4	0.0
Se	0.7	−1.8

Table 3 Calculated UBDE values for the series of {Mes*P=C(Cl)–P(=X)(i-Pr)$_2$}AuCl complexes involving either the P(III) → Au or X → Au bonds (X = O, S and Se)

	Complex formed *via* P(III) → Au bonds	Complex formed *via* X → Au bonds
X	UBDE value (kcal mol^{-1})	
O	54.6	42.1
S	54.3	53.9
Se	54.4	54.9

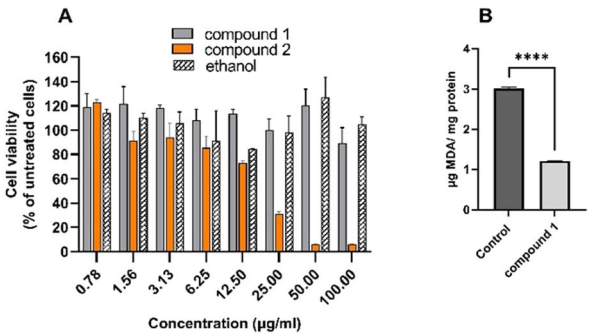

Fig. 2 (A) The effects of compounds **1** and **2** on the viability of B16F10 melanoma cells. Cells were treated with different concentrations of **1** and **2** for 24 h. The corresponding volumes of ethanol used as vehicle were also tested. (B) Quantification of MDA levels in the cells treated with 100 µg mL^{-1} of derivative **1** for 24 h were determined by HPLC. Untreated cells were used as controls****, $p \leq$ 00 001.

Hz). The NMR spectra as well as the HRMS data are presented experimental part. The molecular structure of **3** in solid state was unambiguously determined by single crystal X-ray diffraction (Fig. 1 (right) and SI for supplementary crystallographic data). Compound **3** crystallizes in the orthorhombic *Pnma* space group as a solvate with one dichloromethane molecule. The geometrical parameters for compound **3** (see Table S4 in SI) are similar to those observed for the Pd complex of the analogue P═S ligand.[11] The Pd–Se bond length in **3** (2.398(1)Å) is in a similar range as previously reported in the literature for such bond.[22–24] Theoretical explorations of **3** and its counterparts containing O and S were conducted to assess their thermal accessibility, and the strength of X → Pd (X = O, S, Se) and P(III) → Pd bonds. Based on the $\Delta_r G$ values, computed for the Mes*P═C(Cl)–P(═X)(i-Pr)$_2$ + Pd(COD)Cl$_2$ ⇌ {Mes*P═C(Cl)–P(═X)(i-Pr)$_2$}PdCl$_2$ + COD reaction, the stability of targeted chelate complexes increases from O towards Se (see Table S12 and the related discussions in the SI). This is consistent with the UBDE analysis, which suggest a similar tendency for the increasing strength of X → Pd bond (Table S13), and with the NBO data (Tables S14 and S15), given that bond orders rise from O → Pd (BO = 0.23) to S → Pd (BO = 0.42) and Se → Pd (BO = 0.46). Computed NBO charges (Table S14), as well as a detailed discussion regarding the UBDE and NBO data are presented in the SI.

The study of the coordination ability of **1** was extended by connecting it to a copper(II) fragment. The reaction of phosphavinyl(selenoxo)phosphorane **1** with copper(II) acetate monohydrate leads to [{Mes*P═C(Cl)–P(═Se)(i-Pr)$_2$}Cu^{2+}] × 2AcO$^-$ **4**, which is the first reported copper(II) complex containing a phoshavinyl(chalcogenoxo)phosphorane as ligand. The formation of **4** was evidenced in solution by both multinuclear NMR spectroscopy and HRMS spectrometry. Thus, in the ^{31}P NMR spectrum, two doublet signals were observed, one broad at 292.3 ppm attributed to the P(III) phosphorus atom involved in P═C unit and the other one at 71.1 ppm for P(V) atom ($^2J_{P,P}$ = 120.3 Hz). It is worth mentioning that the signal assigned to P(III) atom is upfield shifted in **4** compared to the signal for the same atom in the starting material **1** (the signal for P(III) in **1** is at 336.1 ppm, d, $^2J_{P,P}$ = 95.4 Hz) while the signal for P(V) remains in a close range (69.8 ppm); this suggest the formation of a new coordinative compound involving a P(III) → Cu connection. The presence of a copper atom in compound **4** was supported by HRMS analysis.

Considering the proven versatility of Mes*P═C(Cl)–P(═Se)(i-Pr)$_2$ **1** as a building block to obtain coordinative metallic compounds, a noteworthy application would be the synthesis of heterobimetallic compounds. Thus, since the coordination of the gold atom in {Mes*P═C(Cl)–P(═Se)(i-Pr)$_2$}AuCl **2** is achieved by the selective coordination of the Se atom, the lone pair of the P(sp^2) atom can be exploited. In this regard, the reaction of **2** with copper(II) acetate was tested. The reaction was performed in dichloromethane, at room temperature, and was monitored through NMR experiments. The ^{31}P NMR spectra recorded on the reaction mixture after 4 days reveal the complete transformation of **2** in a major product **5** giving rise to one broad signal at 294 ppm and one doublet signal at 69.1 ppm ($^2J_{P,P}$ = 102.7 Hz). When compared to the gold complex **2**, in which only the Se atom is involved in the coordinate bond (331.4 and 64.1 ppm), a dramatic change in the chemical shift of the signal attributed to the P(sp^2) atom was noticed. Furthermore, this resonance signal is in a similar range with the one observed in the case of [{Mes*P═C(Cl)–P(═Se)(i-Pr)$_2$}Cu^{2+}] × 2AcO$^-$ **4** (292.3 ppm). This strongly suggests the formation of a new heterobimetallic complex species **5**, containing two P═C–P═Se moieties coordinated through P(sp^2) atoms to a cooper centre and trough Se atoms to a gold centre (see proposed structure in Experimental part). The formation of compound **5**, {[Mes*P═C(Cl)–P(═Se)(i-Pr)$_2$]$_2$}CuAu(Cl), is supported by HRMS analysis (see Fig. S33 in SI).

Biological applications

The electronic properties of compound **1** combined with the presence of the selenium atom made it interesting for evaluating its potential biological applications.

We have tested the effect of both **1** and **2** derivatives on the viability of B16F10 melanoma cell line. As shown in Fig. 2A, the compound **1** had no cytotoxic effect on the melanoma cells at the tested concentrations. However, the gold complex **2** has drastically reduced the viability of the melanoma cells by over 90% at the highest concentration tested. Based on these results, only Mes*P═C(Cl)–P(═Se)(i-Pr)$_2$ **1** was selected to determine its antioxidant capacity.

Regarding the effect of **1** on the oxidative stress, our study found that MDA levels in cells treated with derivative **1** were markedly reduced compared to the untreated cells (nearly 70% reduction). Therefore, these results demonstrated that the tested compounds are potent antioxidants in B16F10 melanoma cells.

Conclusions

In summary, phosphavinyl(selenoxo)phosphorane derivative **1**, the first compound incorporating the λ^2 P(III)═C and λ^4 P(V)═Se linkages, was obtained and fully characterized through experimental and theoretical methods. This compound was found to be an excellent ligand to form mono and/or bidentate coordination compounds with Au, Pd and Cu fragments. A systematic DFT investigation, blended with NBO, EDA and UBDE calculations, emphasized that the nature of the chalcogen atom within the P═C–P(═X) unit (X = O, S or Se) governs its coordination behaviour towards AuCl fragments. Specifically, with oxygen, coordination proceeds *via* the P(sp^3) atom, with sulphur, the complex exhibits fluxionality, featuring a rapid AuCl transfer between the S and P(sp^3) atoms, while with selenium, the most stable complex arises from a Se → Au bond. These findings demonstrate that the distinct electronic features modulated by different chalcogens can tailor the reactivity of P═C–P(═X) systems, providing useful insights for the rational design of novel compounds. Thus, subtle changes in electron density and chemical bonding across this molecular framework compose an "electronic story" that links structure to reactivity. The synthesis of a novel copper complex involving

a phosphavinyl(chalcogenoxo)phosphorane it is also highlighted, featuring the first representative of its class. Additionally, a novel heterobimetallic complex containing two *d*-block elements (Au and Cu) stabilised with two phospha(selenoxo) phosphorane units was obtained.

Notably, compound **1** may exert beneficial antioxidant effects by reducing oxidative stress without compromising cell viability, highlighting its potential as a protective agent in cellular systems.

Experimental part

General consideration

All synthesis were carried out under an inert atmosphere of argon using Schlenk techniques. Derivative Mes*P═C(Cl)–P(i-Pr)$_2$ was obtained by a procedure previously reported by our group.[11] Toluene, pentane and hexane were used after purification by an automatic purification system of solvents MBRAUN SBS-800. The other chemicals were purchased and used without other purification. NMR spectra were performed on a Bruker Avance 400 MHz spectrometer at the following frequencies: 400.13 MHz for ^{1}H, 100.62 MHz for ^{13}C, 162.00 MHz for ^{31}P, 76.31 MHz for ^{77}Se, and on a Bruker Avance 600 MHz spectrometer: ^{1}H (600.13 MHz), ^{13}C (150.92 MHz), ^{31}P (242.97 MHz) with TMS and H_3PO_4 as references for ^{1}H, ^{13}C and ^{31}P respectively and Me_2Se for ^{77}Se. All spectra were recorded and calibrated using $CDCl_3$ as deuterated solvent. An LTQ Orbitrap XL mass spectrometer (ThermoScientific) was used to record high resolution mass spectra using electrospray ionization.

Synthesis of Mes*P═C(Cl)–P(═Se)(i-Pr)$_2$ (1). To a solution of Mes*P═C(Cl)–P(i-Pr)$_2$ (0.61 g, 1.39 mmol) in 20 mL toluene an excess of selenium (0.22 g, 2.78 mmol) was added, and the mixture was heated under reflux. After 4 h, the reaction mixture was filtered off and the solvent was removed under reduced pressure. Recrystallization in pentane and toluene, at low temperature, lead to the formation of compound **1** as yellow crystals. (0.58 g, 80%)

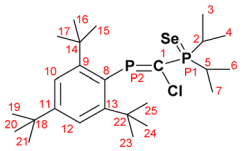

^{1}H NMR ($CDCl_3$, 400.13 MHz): δ (ppm) = 1.21, dd, $^3J_{P,H}$ = 17.9 Hz, $^3J_{H,H}$ = 7.0 Hz and 1.29–1.35, m, 12H, CH_3-*iso*-propyl; 1.33, s, 9H, CH_3-*para-tert*-butyl; 1.47, s, 18H, CH_3-*ortho-tert*-butyl; 2.54–2.67, m, 2H, CH-*iso*-propyl; 7.43, s, 2H, H_{arom}-Mes*.

^{13}C NMR ($CDCl_3$, 100.62 MHz): δ (ppm) = 17.0, 17.6, 17.7, C_3, C_4, C_6, C_7; 28.8, dd, $^1J_{P,C}$ = 50.4 Hz, $^3J_{P,C}$ = 2.1 Hz, C_2, C_5; 31.4, C_{19}–C_{21}; 33.4, d, $^4J_{P,C}$ = 7.4 Hz, C_{15}–C_{17}, C_{23}–C_{25}; 35.1, C_{18}; 38.0, C_{14}, C_{22}; 122.7, 134.9, dd, C_8, $^1J_{P,C}$ = 65.1 Hz, $^3J_{P,C}$ = 13.6 Hz, C_{10}, C_{12}; 151.2, C_{11}; 152.7, dd, $^1J_{P,C}$ = 81.3 Hz, $^1J_{P,C}$ = 32.6 Hz, C_1; 153.5 and 153.6, C_9, C_{13}.

^{31}P{^{1}H} NMR ($CDCl_3$, 162.00 MHz): δ (ppm) = 69.8, d, $^2J_{P,P}$ = 95.4 Hz, $^1J_{P,Se}$ = 707.9 Hz (sat), P_1; 336.1, d, $^2J_{P,P}$ = 95.4 Hz, $^3J_{P,Se}$ = 61.3 Hz (sat), P_2.

^{77}Se{^{1}H} NMR ($CDCl_3$, 76.31 MHz): δ (ppm) = −408.8, dd, $^1J_{P,Se}$ = 707.9 Hz, $^3J_{P,Se}$ = 61.3 Hz, Se.

HRMS (ESI): $C_{25}H_{43}ClP_2Se$ calcd. $[M + 1]^+$: 521.17665; found 521.17426.

Synthesis of {Mes*P═C(Cl)–P(═Se)(i-Pr)$_2$}AuCl (2). A solution of Mes*P═C(Cl)–P(═Se)(i-Pr)$_2$ **1** (0.6 g, 1.15 mmol) in 7 mL CH_2Cl_2 was added to Au(SMe_2)Cl (0.34 g,1.15 mmol) at room temperature. After 30 minutes of stirring, the volatiles were removed under low pressure and derivative **2** was obtained as a yellow powder. (0.83 g, 95%)

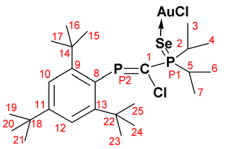

^{1}H NMR ($CDCl_3$, 400.13 MHz): δ (ppm) = 1.26, dd, $^3J_{P,H}$ = 18.3 Hz, $^3J_{H,H}$ = 7.0 Hz and 1.38, dd, $^3J_{P,H}$ = 18.9 Hz, $^3J_{H,H}$ = 7.0 Hz, 12H, CH_3-*iso*-propyl; 1.34, s, 9H, CH_3-*para-tert*-butyl; 1.48, s, 18H, CH_3-*ortho-tert*-butyl; 2.65–2.77, m, 2H, CH-*iso*-propyl; 7.45, s, 2H, H_{arom}-Mes*.

^{13}C NMR ($CDCl_3$, 100.62 MHz): δ (ppm) = 16.9, 17.5, 17.53, C_3, C_4, C_6, C_7; 28.8, d, $^1J_{P,C}$ = 41.1 Hz, C_2, C_5; 31.2, C_{19}–C_{21}; 33.3, d, $^4J_{P,C}$ = 6.7 Hz, C_{15}–C_{17}, C_{23}–C_{25}; 35.0, C_{18}; 37.9, C_{14}, C_{22}; 122.8, C_{10}, C_{12}; 133.3, dd, $^1J_{P,C}$ = 62.8 Hz, $^3J_{P,C}$ = 10.8 Hz, C_8; 150.6, dd, $^1J_{P,C}$ = 76.1 Hz, $^1J_{P,C}$ = 34.8 Hz, C_1; 151.5, C_{11}; 153.6, d, $^3J_{P,C}$ = 2.5 Hz, C_9, C_{13}.

^{31}P{^{1}H} NMR ($CDCl_3$, 162.00 MHz): δ (ppm) = 64.1, d, $^2J_{P,P}$ = 92.0 Hz, $^1J_{P,Se}$ = 664.2 Hz (sat), P_1; 331.4, d, $^2J_{P,P}$ = 92.0 Hz, $^3J_{P,Se}$ = 71.6 Hz (sat), P_2.

^{77}Se{^{1}H} NMR ($CDCl_3$, 76.31 MHz): δ (ppm) = −377.7, d broad, $^1J_{P,Se}$ = 664.2 Hz, Se.

HRMS (ESI): $C_{25}H_{43}AuCl_2P_2Se$ calcd. [2 M–AuCl–Cl]$^+$: 1237.30475; found 1237.30798.

Synthesis of {Mes*P═C(Cl)–P(═Se)(i-Pr)$_2$}PdCl$_2$ (3). A solution of **1** (120 mg, 0.23 mmol) and dichloro(1,5-cyclooctadiene) palladium(II) (70 mg, 0.23 mmol) in CH_2Cl_2 (7 mL) was stirred, at room temperature, for 30 minutes. After removal of volatile compounds under vacuum, compound **3** was obtained as orange crystals, in hexane: toluene 1 : 1 vol, at −20 °C. (131 mg, 81%)

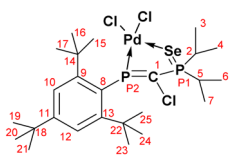

^{1}H NMR ($CDCl_3$, 600.13 MHz): δ (ppm) = 1.32, s, 9H, CH_3-*para-tert*-butyl; 1.36, dd, $^3J_{P,H}$ = 19.3 Hz, $^3J_{H,H}$ = 7.0 Hz and 1.43, dd, $^3J_{P,H}$ = 20.2 Hz, $^3J_{H,H}$ = 7.0 Hz, 12H, CH_3-*iso*-propyl; 1.69, s, 18H, CH_3-*ortho-tert*-butyl; 2.68–2.74, m, 2H, CH-*iso*-propyl; 7.57, d, $^4J_{P,H}$ = 4.3 Hz, 2H, H_{arom}-Mes*.

^{13}C NMR ($CDCl_3$, 150.92 MHz): δ (ppm) = 17.1–17.3, m, C_3, C_4, C_6, C_7; 28.1–28.5, m, C_2, C_5; 31.0–31.1, m, C_{19}–C_{21}; 35.2–35.5, m, C_{15}–C_{18}, C_{23}–C_{25}; 39.6, C_{14}, C_{22}; 118.5, dd, $^1J_{P,C}$ = 7.5 Hz, $^3J_{P,C}$

= 10.2 Hz, C_8; 125.6, t, $^3J_{P,C}$ = 9.5 Hz, C_{10}, C_{12}; 135.6, dd, $^1J_{P,C}$ = 42.0 Hz, $^1J_{P,C}$ = 23.9 Hz, C_1; 155.4, d, $^2J_{P,C}$ = 3.8 Hz, C_9, C_{13}.

$^{31}P\{^1H\}$ NMR ($CDCl_3$, 242.97 MHz): δ (ppm) = 64.1, d, $^2J_{P,P}$ = 76.3 Hz, $^1J_{P,Se}$ = 526.2 Hz, P_1; 284.0, d, $^2J_{P,P}$ = 76.3 Hz, P_2.

$^{77}Se\{^1H\}$ NMR ($CDCl_3$, 76.31 MHz): δ (ppm) = −103.2, dd, $^1J_{P,Se}$ = 526.2 Hz, $^3J_{P,Se}$ = 21.9 Hz, Se.

HRMS (ESI): $C_{25}H_{43}Cl_3PdP_2Se$ calcd. $[M + Na]^+$: 718.99978, found 718.99786; calcd $[2\ M + Na]^+$ 1417.00859, found 1417.01538.

Synthesis of [{Mes*P═C(Cl)–P(═Se)(i-Pr)$_2$}Cu^{2+}] × 2 AcO$^-$ (4). Copper(II) acetate monohydrate (110 mg, 0.57 mmol) was added to a solution of **1** (300 mg, 0.57 mmol) in toluene (5 mL) and the reaction mixture was stirred, at room temperature. After 4 days the volatiles of the resulting dark brown solution were removed under low pressure, and the resulting solid was washed with pentane. Compound **4** was obtained as a dark red solid from toluene, at low temperature. (113 mg, 76%)

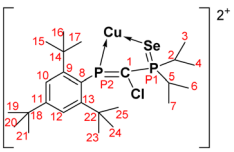

^1H NMR ($CDCl_3$, 600.13 MHz): δ (ppm) = 1.24, dd, $^3J_{P,H}$ = 18.7 Hz, $^3J_{H,H}$ = 7.0 Hz, 6H, CH_3-*iso*-propyl; 1.33, s, 9H, CH_3-*para-tert*-butyl; 1.42, dd, $^3J_{P,H}$ = 19.5 Hz, $^3J_{H,H}$ = 7.0 Hz, 6H, CH_3-*iso*-propyl; 1.52, s, 18H, CH_3-*ortho-tert*-butyl; 2.78, h, 2H, CH-*iso*-propyl; 7.47, s, 2H, H_{arom}-Mes*.

^{13}C NMR ($CDCl_3$, 154.97 MHz): δ (ppm) = 17.1, 17.4, C_3, C_4, C_6, C_7; 28.6, d, $^1J_{P,C}$ = 39.2 Hz, C_2, C_5; 31.3, C_{19}–C_{21}; 34.1, d, $^4J_{P,C}$ = 3.3 Hz, C_{15}–C_{17}, C_{23}–C_{25}; 35.3, C_{18}; 38.4, C_{14}, C_{22}; 123.8, C_{10}, C_{12}; 125.4, dd, $^1J_{P,C}$ = 40.1 Hz, $^3J_{P,C}$ = 11.4 Hz, C_8; 153.2, C_{11}; 155.0, C_9, C_{13}.

$^{31}P\{^1H\}$ NMR ($CDCl_3$, 162.00 MHz): δ (ppm) = 71.1, d, $^2J_{P,P}$ = 120.3 Hz, P_1; 292.3, d broad, P_2.

HRMS (ESI): $C_{50}H_{86}Cl_2CuP_4Se_2$ calcd. $[2\ M\text{-}Cu\text{-}2xOAc]^+$: 1103.26780; found 1103.27515.

Synthesis of {[Mes*P═C(Cl)–P(═Se)(i-Pr)$_2$]$_2$}CuAu(Cl) (5). Copper(II) acetate monohydrate (70 mg, 0.35 mmol) was added to a solution of **2** (260 mg, 0.35 mmol) in CH_2Cl_2 (5 mL) and the reaction mixture was stirred, at room temperature. After 4 days the volatiles of the resulting dark brown solution were removed under low pressure, and the resulting solid was washed with toluene. Compound **5** was obtained as a dark red solid from toluene, at room temperature. (320 mg, 70%)

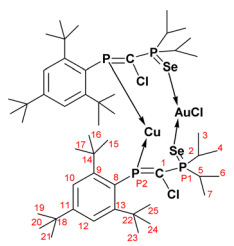

^1H NMR ($CDCl_3$, 400.13 MHz): δ (ppm) = 1.28, dd, $^3J_{P,H}$ = 18.8 Hz, $^3J_{H,H}$ = 6.9 Hz, 6H, CH_3-*iso*-propyl; 1.34, s, 9H, CH_3-*para-tert*-butyl; 1.45, dd, $^3J_{P,H}$ = 19.8 Hz, $^3J_{H,H}$ = 6.9 Hz, 6H, CH_3-*iso*-propyl; 1.54, s, 18H, CH_3-*ortho-tert*-butyl; 2.81, h, 2H, CH-*iso*-propyl; 7.49, s, 2H, H_{arom}-Mes*.

^{13}C NMR ($CDCl_3$, 100.62 MHz): δ (ppm) = 17.2, 17.4, 17.5, C_3, C_4, C_6, C_7; 28.7, d, $^1J_{P,C}$ = 38.3 Hz, C_2, C_5; 31.2, C_{19}–C_{21}; 34.1, d, $^4J_{P,C}$ = 3.6 Hz, C_{15}–C_{17}, C_{23}–C_{25}; 35.2, C_{18}; 38.4, C_{14}, C_{22}; 123.6, d broad, C_{10}, C_{12}; 153.0, C_{11}; 1554.8, C_9, C_{13}.

$^{31}P\{^1H\}$ NMR ($CDCl_3$, 162.00 MHz): δ (ppm) = 69.1, d, $^2J_{P,P}$ = 102.7 Hz, P_1; 294, d broad, P_2.

HRMS (ESI): $C_{50}H_{86}AuCl_3CuP_4Se_2$ calcd. $[M]^+$: 1335.20320; found 1335.20056.

X-ray data. Crystal structure determination. Single crystals of Mes*P═C(Cl)–P(═Se)(i-Pr)$_2$ **1**, {Mes*P═C(Cl)–P(═Se)(i-Pr)$_2$}AuCl **2** and {Mes*P═C(Cl)–P(═Se)(i-Pr)$_2$}$PdCl_2$ **3** were obtained at low temperature by vapor diffusion between a hexane solution of the respective compound and toluene (for **1** and **3**) and chloroform for **2**. The crystals of **1–3**, were mounted on MiTeGen microMounts cryoloops and data were collected on a Bruker D8 VENTURE diffractometer using Mo-Kα radiation (λ = 0.71073 Å) from a IμS 3.0 micro focus source with multilayer optics, at low temperature (100 K). For structure solving and refinement the Bruker APEX5 software package was used.[25] The structures were solved by dual methods (SHELXT-2018/2)[26] and refined by full matrix least-squares procedures based on F^2 with all measured reflections (SHELXL-2019/1).[27] The structures were refined with anisotropic thermal parameters for non-H atoms. Hydrogen atoms were placed in fixed, idealized positions and refined with a riding model and a mutual isotropic thermal parameter.

In the case of compound **2** the measured crystal was of low quality. The structure could be solved partially, but anisotropic refinement results in some atoms having NPD (non-positive definite) thermal ellipsoids. Additional spherical absorption correction with several different values were tested to try to alleviate this problem but without success. Consequently, final solution and refinement to convergence was not possible and the data was not deposited in the CSD. No other crystals could be measured so far.

Further details on the data collection and refinement methods can be found in Table S1. The drawings were created with the Diamond program.[28]

Computational details and methodology

Geometry optimization and vibrational analyses. All calculations were performed within the framework of the Density Functional Theory (DFT), using the Gaussian 16 software package.[29] The molecular geometries of investigated systems were fully optimized in the gaseous phase without any symmetry constraints, with the optimization criteria being set to tight. In several cases, the molecular geometries were additionally optimized in dichloromethane (DCM), employing the SMD[30] variation of the polarizable continuum solvation model (for DCM, ε = 8.93). The PBE0 hybrid functional developed by Adamo and Barone,[31] and Dunning's cc-pVTZ valence triple-zeta quality basis set,[32–36] were employed in all DFT calculations. For the gold and palladium atoms, the relativistic core electrons

were replaced by effective core potentials (ECPs), as implemented in the cc-pVTZ-PP basis set. More precisely, for the Pd atom the employed Stuttgart-Cologne pseudopotential (PP) replaces the inner 28 core electrons leaving the outer 18 electrons to be treated explicitly in the calculation (*i.e.*, the ECP28MDF Pd-ECP),[37] while for the Au atom it replaces the inner 60 electrons leaving 19 valence electrons to be treated explicitly (*i.e.*, the ECP60MDF Au-ECP).[38] The equilibrium geometries calculated for the investigated compounds closely match the solid-state structures, supporting the current choice of the DFT level of theory. This is reinforced by previous theoretical investigations carried out on similar molecular systems and their metal complexes,[11,12,16] which emphasized that hybrid DFT methods combined with valence triple-zeta basis sets accurately reproduce and validate experimental data. In all DFT calculations performed herein on the Au(I) and Pd(II) complexes, a singlet spin state was employed, consistent with the expected behaviour of d^{10} metals in linear geometries and d^8 metals in square-planar geometries. Vibrational analyses were carried out to characterize the nature of the stationary points. Frequency calculations were also used to compute Gibbs free energies within the framework of the harmonic oscillator approximation for vibrational contribution (further details regarding the thermodynamic equations are available in ref. 39). The integration grid employed in all calculations performed herein was of 99 radial shells and 950 angular points for each shell (99 950), known as the "ultrafine" grid in Gaussian 16.

EDA calculations. The Energy Decomposition Analysis (EDA) scheme, proposed by Li and Su,[40] has been employed to compute the interaction energies of the coordinate bonds formed between the Mes*P═C(Cl)–P(═X)(i-Pr)$_2$ system (X = O, S, Se) and the AuCl and $PdCl_2$ moieties. Within this technique the energy difference is decomposed as follows:

$$\Delta E_{DFT} = \Delta E_{ele} + \Delta E_{ex\text{-}rep} + \Delta E_{orb} + \Delta E_{cor}$$

where ΔE_{ele} is the electrostatic energy, $\Delta E_{ex\text{-}rep}$ the difference between exchange and repulsions ΔE_{orb} the orbital relaxation (*i.e.*, the polarization energy), and ΔE_{cor} the correlation energy. EDA calculations were performed in Turbomole software package (version 7.7).[41] The wavefunctions of the Gaussian optimized structures were calculated using RI-DFT.[42–45] The hybrid functional and basis sets employed in the Turbomole calculations are the same as those used in Gaussian 16 for geometry optimizations, namely the PBE0 functional and cc-pVTZ basis set (cc-pVTZ-PP, for Au and Pd), as implemented in Turbomole. For computing the integrals, a grid-size of 5 was employed in all Turbomole calculations.

UBDE calculations. The unrelaxed heterolytic bond dissociation energy (UBDE) values of the investigated coordinate bonds were computed as the difference between the energies of {Mes*P═C(Cl)–P(═X)(i-Pr)$_2$}AuCl and {Mes*P═C(Cl)–P(═X)(i-Pr)$_2$}$PdCl_2$ complexes and the resulting fragments obtained by breaking the P(III) → M and/or X → M bonds (X = O, S, Se; M = Au, Pd). Within the current unrelaxed approximation, the energy of the investigated fragments was determined through single-point calculations, without any subsequent geometry optimizations. The UBDE values are calculated with the following formula:

$$UBDE = E_{complex} - E_{fragment\_1} - E_{fragment\_2}$$

where E represents the electronic energies of the complex and its resulting fragments, without ZPE or thermal free energy corrections included.

NBO calculations. Natural Bond Orbital (NBO)[46–48] analyses were carried out on the optimized structures of the investigated species. Natural charges were computed within the framework of the Natural Population Analysis (NPA) of the NBO theory,[49] while bond orders were calculated within Natural Resonance Theory (NRT) analysis.[50–52] All these calculations were performed using the NBO7.0 program.[53]

Biologic activity of derivative 1 and 2

Materials and methods

Cell line. Murine melanoma cells B16.F10 (ATCC, CRL-6475) were cultured in Dulbecco's modified Eagle's medium (DMEM, Biowest), as described previously.[54]

Cell viability assay. To determine the effects of derivative **1** and **2** on tumour cell viability, the B16.F10 melanoma cells (10 000 cells per well) were seeded in a 96-well plate and allowed to attach to the plate overnight. Next day, different concentrations of both **1** and **2** derivatives solubilized in ethanol as well as ethanol alone, were added to the appropriate wells. As controls, we used cells grown in the appropriate culture media. All samples and controls were tested in triplicate. After 24 hours, cell viability was quantified using WST-1 reagent according to the manufacturer instructions (Roche, # RO05015944001). Results were expressed as the percentage of cell viability relative to the control.

Determination of malondialdehyde levels. To investigate whether the phosphavinyl(selenoxo)phosphorane **1** can affect oxidative stress in melanoma cells, we determined the concentration of malondialdehyde (MDA) – a marker for membrane lipid peroxidation, in tumour cell lysate through high-performance liquid chromatography (HPLC). B16F10 cells were treated with 100 μg ml^{-1} of **1** in ethanol. After 24 hours, the cells were lysed using RIPA cell lysis buffer (Millipore, Germany). Before HPLC analysis of MDA, sample deproteinization was performed as described previously,[55] and 100 μl of each supernatant was used for HPLC analysis. The column type was Mediterranea Sea18 Column 5 μm 25 × 0.46 cm (Teknokroma, Spain) and the mobile phase consisted of 30 mM KH2PO4/methanol in a volume ratio of 65 : 35. Flow rate was set at 1 mL min^{-1} and MDA was measured using a UV detector set at 254 nm. The retention time of MDA was about 3.16 min. Data were expressed as μg of MDA per mg of protein in cell lysate. Each sample was determined in triplicate.

Statistical analysis. Data from different experiments were reported as mean ± SD. Student's *t*-test for independent means was performed to analyse the MDA data, using GraphPad Prism9 software (San Diego, CA). A *P* value of <05 was considered significant.

Author contributions

The manuscript was written through contributions of all authors. All authors have given approval to the final version of the manuscript.

Conflicts of interest

The authors declare no conflicts of interest.

Data availability

The data supporting this article have been included as part of the supplementary information (SI). Supplementary information is available. See DOI: https://doi.org/10.1039/d5ra05176b.

CCDC 2448919 (**1**) and 2448920 (**3**) contain the supplementary crystallographic data for this paper.[56a,b]

Acknowledgements

The computational resources provided by the high-performance computational facility of the Babes-Bolyai University (MADECIP, POSCCE, COD SMIS 48801/1862) are acknowledged.

Notes and references

1 J. Escudie and H. Ranaivonjatovo, *Organometallics*, 2007, **26**, 1542–1559.
2 A. Ziółkowska, J. Doroszuk and Ł. Ponikiewski, *Organometallics*, 2023, **42**, 505–537.
3 K. Nishide, H. Liang, S. Ito and M. Yoshifuji, *J. Organomet. Chem.*, 2005, **690**, 4809–4815.
4 S. Ito, H. Liang and M. Yoshifuji, *Chem. Commun.*, 2003, 398–399.
5 S. Ito and M. Yoshifuji, *Chem. Commun.*, 2001, 1208–1209.
6 S. Ito, H. Liang and M. Yoshifuji, *J. Organomet. Chem.*, 2005, **690**, 2531–2535.
7 S. Ito, K. Nishide and M. Yoshifuji, *Organometallics*, 2006, **25**, 1424–1430.
8 H. Liang, S. Ito and M. Yoshifuji, *Org. Biomol. Chem.*, 2003, **1**, 3054–3058.
9 H. Liang, K. Nishide, S. Ito and M. Yoshifuji, *Tetrahedron Lett.*, 2003, **44**, 8297–8300.
10 H. Liang, S. Ito and M. Yoshifuji, *Org. Lett.*, 2004, **6**, 425–427.
11 I.-A. Aghion, R. Septelean, A.-C. Tomut, I.-T. Moraru, A. Soran and G. Nemes, *Organometallics*, 2024, **43**, 2062–2076.
12 A.-C. Tomut, I.-A. Aghion, R. Septelean, I. D. Porumb, I.-T. Moraru and G. Nemes, *RSC Adv.*, 2024, **14**, 10161–10171.
13 R. Septelean, G. Nemes, J. Escudié, I. Silaghi Dumitrescu, H. Ranaivonjatovo, P. Petrar, H. Gornitzka, L. Silaghi-Dumitrescu and N. Saffon, *Eur. J. Inorg. Chem.*, 2009, **2009**, 628–634.
14 R. Septelean, H. Ranaivonjatovo, G. Nemes, J. Escudié, I. Silaghi-Dumitrescu, H. Gornitzka, L. Silaghi-Dumitrescu and S. Massou, *Eur. J. Inorg. Chem.*, 2006, **2006**, 4237–4241.
15 M. Yoshifuji, *J. Organomet. Chem.*, 2000, **611**, 210–216.
16 R. Septelean, A. Muresan, A. Soran, I.-T. Moraru and G. Nemes, *Rev. Roum. Chim.*, 2020, **65**, 579–585.
17 M. Jorges, S. Mondal, M. Kumar, F. Krischer, J. Loffler and V. Gessner, *Organometallics*, 2024, **43**, 585–593.
18 J. D. E. T. Wilton-Ely, A. Schier and H. Schmidbaur, *Inorg. Chem.*, 2001, **40**, 11788–11798.
19 J. Konu, H. M. Tuononen and T. Chivers, *Inorg. Chem.*, 2009, **48**, 11788–11798.
20 P. G. Jones and B. Ahrens, *Chem. Commun.*, 1998, 2307–2308.
21 V. Cadierno, J. Diez, J. Garcia-Alvarez and J. Gimeno, *Dalton Trans.*, 2010, **39**, 941–956.
22 R. S. Chauhan, G. Kedarnath, A. Wadawale, A. M. Z. Slawinb and V. K. Jain, *Dalton Trans.*, 2013, **42**, 259–269.
23 R. Gonzalez, R. Azpiroz, P. Sharma, C. P. Villamizar, B. Anzaldo, F. J. Pérez-Flores and R. A. Toscano, *Inorg. Chim. Acta*, 2020, **506**, 119531.
24 R. Bhatt, A. K. Sharma, N. B. Himanshi and H. Joshi, *Polyhedron*, 2020, **185**, 114597.
25 APEX5, *v.2023.9.2*, Bruker AXS Inc., Madison, Wisconsin, USA, 2023.
26 G. M. Sheldrick, *Acta Crystallogr. A*, 2015, **71**, 3–8.
27 G. M. Sheldrick, *Acta Crystallogr. C*, 2015, **71**, 3–8.
28 H. Putz and K. Brandenburg, *DIAMOND - Crystal and Molecular Structure Visualization, Crystal Impact GbR*, Kreuzherrenstr, 53227 Bonn, Germany, 2021, 102.
29 M. J. Frisch, G. W. Trucks, H. B. Schlegel, G. E. Scuseria, M. A. Robb, J. R. Cheeseman, G. Scalmani, V. Barone, G. A. Petersson, H. Nakatsuji, X. Li, M. Caricato, A. V. Marenich, J. Bloino, B. G. Janesko, R. Gomperts, B. Mennucci, H. P. Hratchian, J. V. Ortiz, A. F. Izmaylov, J. L. Sonnenberg, D. Williams-Young, F. Ding, F. Lipparini, F. Egidi, J. Goings, B. Peng, A. Petrone, T. Henderson, D. Ranasinghe, V. G. Zakrzewski, J. Gao, N. Rega, G. Zheng, W. Liang, M. Hada, M. Ehara, K. Toyota, R. Fukuda, J. Hasegawa, M. Ishida, T. Nakajima, Y. Honda, O. Kitao, H. Nakai, T. Vreven, K. Throssell, J. A. Jr. Montgomery, J. E. Peralta, F. Ogliaro, M. J. Bearpark, J. J. Heyd, E. N. Brothers, K. N. Kudin, V. N. Staroverov, T. A. Keith, R. Kobayashi, J. Normand, K. Raghavachari, A. P. Rendell, J. C. Burant, S. S. Iyengar, J. Tomasi, M. Cossi, J. M. Millam, M. Klene, C. Adamo, R. Cammi, J. W. Ochterski, R. L. Martin, K. Morokuma, O. Farkas, J. B. Foresman and D. J. Fox, *Gaussian 16, Revision C.01*, Gaussian, Inc., Wallingford CT, 2016.
30 A. V. Marenich, C. J. Cramer and D. G. Truhlar, *J. Phys. Chem. B*, 2009, **113**, 6378–6396.
31 C. Adamo and V. Barone, *J. Chem. Phys.*, 1999, **110**, 6158–6170.
32 T. H. Dunning Jr, *J. Chem. Phys.*, 1989, **90**, 1007–1023.
33 R. A. Kendall, T. H. Dunning Jr and R. J. Harrison, *J. Chem. Phys.*, 1992, **96**, 6796–6806.
34 D. E. Woon and T. H. Dunning Jr, *J. Chem. Phys.*, 1993, **98**, 1358–1371.
35 K. A. Peterson, D. E. Woon and T. H. Dunning Jr, *J. Chem. Phys.*, 1994, **100**, 7410–7415.
36 A. K. Wilson, T. van Mourik and T. H. Dunning Jr, *J. Mol. Struct. (Theochem)*, 1996, **388**, 339–349.

37 K. A. Peterson, D. Figgen, M. Dolg and H. Stoll, *J. Chem. Phys.*, 2007, **126**, 124101.
38 D. Figgen, G. Rauhut, M. Dolg and H. Stoll, *Chem. Phys.*, 2005, **311**, 227–244.
39 D. A. McQuarrie, J. D. Simon, *Molecular Thermodynamics*, Univ. Science Books, Sausalito, CA, 1999.
40 P. Su and H. Li, *J. Chem. Phys.*, 2009, **131**, 014102.
41 R. Ahlrichs, M. Bär, M. Häser, H. Horn and C. Kölmel, *Chem. Phys. Lett.*, 1989, **162**, 165–169.
42 K. Eichkorn, O. Treutler, H. Öhm, M. Häser and R. Ahlrichs, *Chem. Phys. Lett.*, 1995, **240**, 283–290.
43 K. Eichkorn, O. Treutler, H. Öhm, M. Häser and R. Ahlrichs, *Chem. Phys. Lett.*, 1995, **242**, 652–660.
44 K. Eichkorn, F. Weigend, O. Treutler and R. Ahlrichs, *Theor. Chem. Acc.*, 1997, **97**, 119–124.
45 F. Weigend, *Phys. Chem. Chem. Phys.*, 2006, **8**, 1057–1065.
46 F. Weinhold, C. R. Landis, *Valency and Bonding A Natural Bond Orbital Donor-Acceptor Perspective*, Cambridge Univ. Press, Cambridge, UK, 2005.
47 F. Weinhold, C. R. Landis, *Discovering Chemistry with Natural Bond Orbitals*, Wiley-Interscience, Hoboken, NJ, 2012.
48 F. Weinhold, C. R. Landis and E. D. Glendening, *Int. Rev. Phys. Chem.*, 2016, **35**, 399–440.
49 A. E. Reed, R. B. Weinstock and F. Weinhold, *J. Chem. Phys.*, 1985, **83**, 735–746.
50 E. D. Glendening and F. Weinhold, *J. Comput. Chem.*, 1998, **19**, 593–609.
51 E. D. Glendening and F. Weinhold, *J. Comput. Chem.*, 1998, **19**, 610–627.
52 E. D. Glendening, J. K. Badenhoop and F. Weinhold, *J. Comput. Chem.*, 1998, **19**, 628–646.
53 E. D. Glendening, J. K. Badenhoop, A. E. Reed, J. E. Carpenter, J. A. Bohmann, C. M. Morales, P. Karafiloglou, C. R. Landis, F. Weinhold, *NBO 7.0., Theoretical Chemistry Institute*, University of Wisconsin, Madison, 2018.
54 E. Licarete, A. Sesarman, V. F. Rauca, L. Luput, L. Patras and M. Banciu, *Oncol. Lett.*, 2017, **13**, 3942–3950.
55 M. Banciu, J. M. Metselaar, R. M. Schiffelers and G. Storm, *Neoplasia*, 2008, **10**, 108–117.
56 (*a*) CCDC 2448919: Experimental Crystal Structure Determination, 2025, DOI: **10.5517/ccdc.csd.cc2n69dl**; (*b*) CCDC 2448920: Experimental Crystal Structure Determination, 2025, DOI: **10.5517/ccdc.csd.cc2n69fm**.